Nationaal Lucht- en Ruimtevaartlaboratorium
National Aerospace Laboratory NLR

NLR-TP-2000-196

Towards Integrated Analysis of Gas Turbine Components for Life Prediction

R. Hagmeijer, A. de Boer, T. Tinga, H.J. ten Hoeve,
H.N. Huisman, J.C. Kok, G.A. Kool, M.F.J. Koolloos,
W.P.J. Visser, S. Woldendorp and W.B. de Wolf

Nationaal Lucht- en Ruimtevaartlaboratorium
National Aerospace Laboratory NLR

NLR-TP-2000-196

Towards Integrated Analysis of Gas Turbine Components for Life Prediction

R. Hagmeijer, A. de Boer, T. Tinga, H.J. ten Hoeve,
H.N. Huisman, J.C. Kok, G.A. Kool, M.F.J. Koolloos,
W.P.J. Visser, S. Woldendorp and W.B. de Wolf

This investigation has been carried out under a contract awarded by the Netherlands Agency for Aerospace Programmes, contract number 01613N.
The Netherlands Agency for Aerospace Programmes has granted NLR permission to publish this report.

The contents of this report may be cited on condition that full credit is given to NLR and the authors.

Division: Structures and Materials
Issued: May 2000
Classification of title: Unclassified

Summary

An overview of the activities on integrated analysis of gas turbine components at the National Aerospace Laboratory NLR in the Netherlands is presented. Key elements are the multi-disciplinary frame-work including Engine System Performance, Fluid Dynamics Analysis, Heat Flow Analysis, Stress Analysis and Life Assessment, and a complementary approach employing Asymptotic Analysis, Computational Analysis and Physical Experiments.

Contents

15 Figures

(40 pages in total)

This page is intentionally left blank.

1 Introduction

In 1996 the project ”Thermo-Mechanical modelling of gas turbine components” was initiated at the National Aerospace Laboratory of the Netherlands (NLR), under a contract awarded by the Netherlands Agency for Aerospace programmes (NIVR).

The objective of the project is to develop, acquire, employ and verify computational and experimental tools which can be used for the analysis and design of coated or non-coated gas turbine components.

A key element of the project is the essentially integrated **Multi-Disciplinary frame-work**, see Fig. 1a, involving five main disciplines:

- **Engine System Performance**, to determine engine performance parameters,
- **Fluid Dynamics Analysis**, to determine aerothermodynamic loads,
- **Heat Flow Analysis**, to determine temperatures,
- **Stress Analysis**, to determine mechanical stresses, and
- **Life Assessment**, to determine life of components.

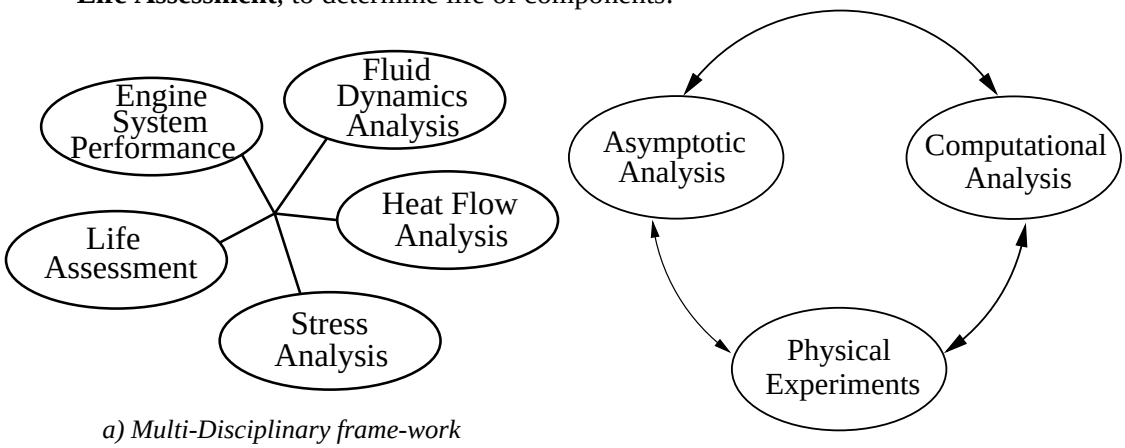

a) Multi-Disciplinary frame-work

b) Complementary Approaches

Fig. 1 Key Elements of Integrated Analysis

Another key element of the project is the **Complementary Approach** employed, see Fig. 1b, involving three approaches:

- **Asymptotic Analysis**, employing assumptions that lead to a reduced complexity of the problem, or, equivalently, to a sub-set of the governing equations. For example one can assume temperature independent conductivity in a heat flow problem. The solution of the reduced problem is exact in the limit of temperature independent conductivity while it is approximate for moderate temperature dependency of the conductivity.

- **Computational Analysis**, employing discrete approximations of the governing equations which are solved numerically.
- **Physical Experiments**.

All of these three approaches are complementary in the sense that different approaches may be used to **verify** correctness, while, alternatively, different approaches may be used to **validate** correlations. For example, a computational analysis algorithm, e.g. a finite element method, may be verified by comparing the solution of a reduced problem to the associated asymptotic analysis solution. Alternatively the same algorithm may be validated by comparison of the solution to data obtained from physical experiments.

The project started with a **pilot study** with the objective to identify which disciplines and associated tools were to be developed, acquired or enhanced. The driving element of the pilot study was to determine the thermo-elastic stresses in an internally cooled cylinder when exposed to a hot gas cross-flow with the objective to provide input data to life prediction assessment.

The work included formal description of the underlying integrated multi-disciplinary problem, subdivision into a number of smaller problems, asymptotic analysis, computational analysis, physical experiments and, finally, synthesis of the study results. The technical areas investigated are:

1. Compressible viscous flow of a hot gas around component(s)
2. Heat transfer from the gas to the component(s)
3. Internal cooling of the component(s)
4. Time-dependent heat flow in the component(s)
5. Time-dependent stress distribution in the component(s)
6. Life assessment of the component(s)

The results of this pilot study were reported to NIVR in a series of NLR contract reports, including a general description of the enveloping project, an inventory of European activities, a list of white spots, an overview of the interest of Dutch industry and a summary of possibilities for collaboration.

As a **follow-up of the pilot study** considerable effort has been directed towards actual solution of problems associated with heat transfer, internal cooling, time-dependent heat flow and stress calculations. Activities in the field of life assessment were initially limited to a literature survey. Thermodynamic engine system performance data are necessary to define the boundary conditions for the processes in a particular component. These depend heavily on the engine operating conditions and are calculated using the NLR Gas turbine Simulation Program (GSP) 16. GSP is a

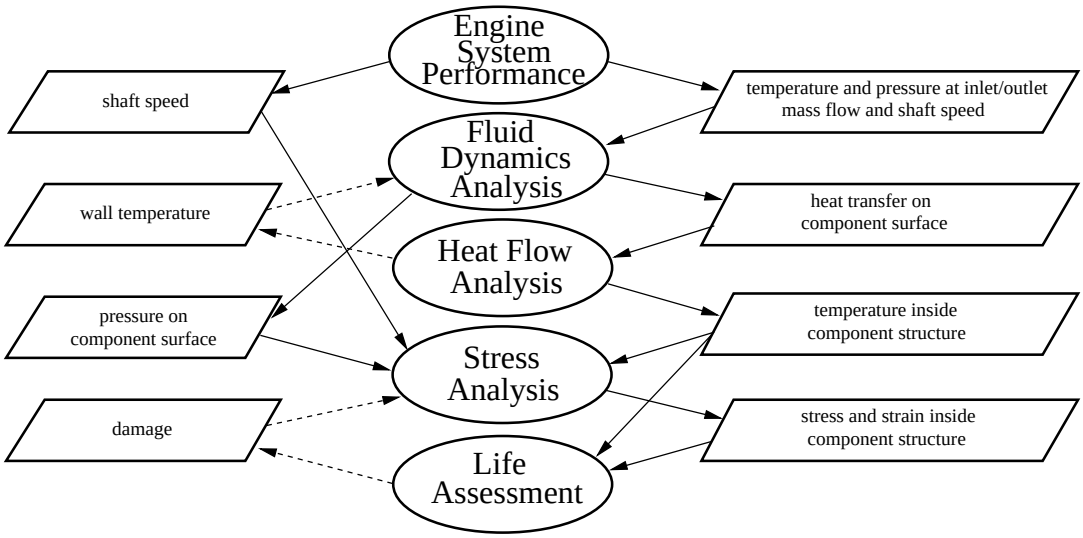

Fig. 2 Interdependencies logic of physical-mathematical sub-problems

generic component based 0/1-dimensional modelling environment for steady-state and transient performance analysis of gas turbine engines.

The present paper globally describes the main achievements of the project ”Thermo-mechanical modelling of gasturbine components” embedded in a functional description of the integrated problem. All five disciplines presented in Fig. 1a are addressed at all three approaches identified in Fig. 1b. Emphasis is put on the interdependency between these discipline in terms of boundary conditions and characteristic time scales and several application examples are presented.

2 Functional Description

The integrated problem investigated can be formulated in terms of a number of sub-problems related to the five disciplines involved, see Fig. 2, while the sub-problems are interacting by the exchange of boundary conditions. It is noted that the dashed arrows in Fig. 2 indicate optional data flows that are not activated yet.

Thermodynamic **Engine System Performance** is calculated using GSP to determine boundary conditions for subsequent analysis of the processes in a particular component, depending on the engine operating conditions. These can be specified using standard reference mission profiles or obtained from in-flight measurements using FACE (ref 12). GSP is necessary to calculate gas parameters at stations for which FACE cannot provide data such as HP turbine inlet temperature,

which normally is not measured by the engine control or monitoring system. Also GSP is able to accurately (with small time steps) calculate transient responses for these parameters (which are critical to engine life) when measure data are not available of have unacceptably high time lags or low update frequencies in FACE.

The conservation laws describing the **Fluid Dynamics Analysis** consist of the Navier-Stokes equations explicitly describing conservation of mass, momentum and energy of gases and liquids. Boundary conditions typically consist of given total pressure and total temperature at inflow boundaries, pressure at subsonic outflow boundaries, and zero slip and wall temperature or zero heat transfer at solid wall boundaries. The boundary conditions at the inflow and outflow boundaries are connected to the Engine System Performance analysis, while the boundary conditions at the solid wall boundaries are connected to the Heat Flow analysis. Solution of the equations provides density, velocity, temperature and pressure distributions in the flow domain and also heat transfer rates at solid wall boundaries.

The conservation law describing the **Heat Flow Analysis** consist of the Fourier heat conduction equation, expressing conservation of energy. Boundary conditions typically consist of initial temperature distribution, temperature prescription on part of the boundary, and heat transfer-rate prescription on part of the boundary. The boundary conditions are connected to the Fluid Dynamics analysis. Solution of the equations provides the temperature distribution inside the component structure.

The conservation laws describing the **Stress Analysis** consist of the Cauchy equations, expressing conservation of momentum. Boundary conditions typically consist of initial stress or displacements distribution, stress prescription on part of the boundary, and temperature distribution. In addition, movement of the component (e.g. rotation) and structural damage may be included. The boundary conditions are connected to the Engine System Performance and the Heat Flow analysis. Solution of the equations provides the stress, strain and displacement distributions inside the component structure.

Once the temperature,stress and strain distributions in the component are known, the final step is to perform **Life Assessment**. This can be done with life prediction models, which either predict the number of cycles to failure or the time to failure. Unlike the fluid dynamics and solid mechanics models, these life prediction models are not analytically derived. Most of the lifing models are based on empirical relations between a certain loading parameter (e.g. stress) and life. As there are several life limiting mechanisms, there is also a variety of lifing models. Examples of

failure mechanisms are fatigue, creep, oxidation and corrosion, as well as combinations of these mechanisms. Each mechanism requires a separate life prediction model.

¿From a dimensional analysis it can be derived that the ratio of the **characteristic time scales** of the heat flow, τ_H, and of the fluid flow, τ_F, respectively, satisfies:

$$\tau_H/\tau_F \sim (\frac{d}{D})^2 Re \frac{\alpha_F}{\alpha_H}, \tag{1}$$

where d is a length scale characterising the thickness of the (plate-) material, D is a length scale characterising the size of the body, Re is the Reynolds number based on D, and:

$$\alpha_H = \frac{k_M}{\rho_M C_M}, \quad \alpha_F = \frac{k}{\rho C_p}, \tag{2}$$

where k, ρ and C denote thermal conductivity, density and specific heat capacity respectively, with M indicating solid material. For typical values of the parameters occuring in Eq.(1) we find for the ratio of characteristic time-scales:

$$\tau_H/\tau_F \gg 1. \tag{3}$$

Hence we conclude that compared to the heat flow problem the fluid dynamics problem can be treated as a quasi-steady-state problem.

This concludes the functional description of the integrated problem. In the next five chapters each of the disciplines involved is addressed in some detail within some or all of the three complementary approaches, while several application examples are presented.

3 Engine System Performance

NLRs Gas turbine Simulation Program (GSP) is a component-based modeling environment for gas turbines. Both steady-state and transient simulation of any kind of gas turbine configuration can

be performed by establishing a specific arrangement of engine component models. GSP calculates gas turbine performance, relative to a reference operating point, usually the design point. Apart from design point analysis, GSP is particularly suitable for off-design analysis. Off-design steady-state and transient performance is calculated using the customary numerical methods of defining engine system states and solving the equations for the conservation of mass, energy and momentum. The component models are non-dimensional, except for the 1-dimensional multi-reactor combustor model. Transient performance is calculated using the quasi steady-state approach (using steady-state component maps), including rotor inertia, heat soakage and component volume effects. For the application of gas turbine component analysis for lifing prediction, model input is formed by operating conditions in terms of flight conditions (speed, pressure altitude, ambient temperature), Power Lever Angle (PLA) or in case the engine control system model is not used: fuel flow and exhaust nozzle area, installation losses such as power off-take (PTO) and customer and/or anti-icing compressor bleed, engine condition/deterioration levels and control mode (full DEEC/FADEC control, back-up control, on ground/in-flight mode etc.). These parameters can be specified using standard reference mission profiles or obtained from in-flight measurements using FACE. Resulting performance data necessary for component analysis are total and static pressures and temperatures, mass flow rates, gas compositions and properties at engine stations before and after the component of interest. For compressors and turbines additional performance data are calculated such as shaft power, compressor bleed flows and turbine cooling flows entering or exiting the proces in the component at a user specified stage. Additional parameters calculated are rotor speed, engine thrust, fuel flows etc.. These may be used for validation against FACE recorded data.

FACE is a measurement system used to monitor both airframe and engine parameters. Engine fuel flows, PLA, nozzle area and flight conditions are sampled at a pre-set time interval and are stored in on-board solid state memory continuously during an entire mission. GSP receives these data as input to calculate detailed engine system performance throughout the mission.

4 Fluid Dynamics Analysis

The present chapter describes the Navier-Stokes equations that govern the Fluid Dynamics problem, as well as the derived asymptotic and numerical analysis methods.

4.1 Navier-Stokes Equations

The Navier-Stokes equations consist of three partial differential equations which express the conservation of mass:

$$\frac{\partial \rho}{\partial t} + \frac{\partial}{\partial x^j}(\rho u^j) = 0, \tag{4}$$

of momentum:

$$\frac{\partial \rho u^i}{\partial t} + \frac{\partial}{\partial x^j}(\rho u^j u^i - \sigma^{ij}) = 0, \quad i = 1, 2, 3, \tag{5}$$

and of energy:

$$\frac{\partial \rho E}{\partial t} + \frac{\partial}{\partial x^j}(\rho u^j H + q^j - \tau^{ij} u^i) = 0. \tag{6}$$

The stress tensor σ^{ij} is the sum of the deviatoric stress tensor τ^{ij} and the mean normal stress tensor $-p\delta^{ij}$:

$$\sigma^{ij} = \tau^{ij} - p\delta^{ij} \tag{7}$$

The heat flux q^j is modeled by the Fourier heat conduction law

$$q^j = -k\frac{\partial T}{\partial x^j}. \tag{8}$$

The system of equations Eq.s (4) to (8) is closed by providing expressions for the static pressure p and the deviatoric stress components τ^{ij} in terms of the conserved variables ρ, ρu^i, and ρE and their gradients.

4.2 Asymptotic Fluid Dynamics Analysis

In section 5.4 an experiment is described involving an internally cooled cylinder instantaneously exposed to a hot gas cross-flow. For this particular problem it is possible to carry out asymptotic analysis of the heat transfer from the external hot gas flow towards the region around the stagnation point and from the cooling channel surface towards the internal gas flow. Both issues are adressed below.

Stagnation region heat transfer. In the near wall limit the Navier-Stokes equations can be approximated by the boundary-layer equations. These boundary-layer equations are transformed by using a Lees-Dorodnitsyn transformation which implies conservation of mass. Then in case of stagnation flow where all inviscid fluid properties except velocity have maxima, the boundary-layer equations for momentum and total enthalpy become ordinary differential equations, see Ref.7 for an excellent overview.

Many authors have solved these equations under various assumptions. The most general solutions probably have been obtained by Fay & Riddell (Ref.4). They have used an extensive set of numerical solutions to correlate the stagnation heat flux algebraically to the Prandtl number, the velocity gradient, and density, viscosity, total enthalpy evaluated both at the wall and at the edge of the boundary-layer. The Fay & Riddel formula can be written as:

$$q_s = B {Pr_w}^{-1} \sqrt{\rho_w \mu_w (\frac{du_e}{dx})_s} (H_e - H_w), \tag{9}$$

with, for the two-dimensional case,

$$B = 0.57\, Pr^{0.4} (\frac{\rho_w \mu_w}{\rho_e \mu_e})^{0.1} \sqrt{\frac{\rho_e \mu_e}{\rho_w \mu_w}}. \tag{10}$$

This formula results in a correlation accuracy of 2% and is frequently applied within the field of hypersonic aerothermodynamics, including flows consisting of callorically imperfect gases or chemical equilibrium mixtures.

The velocity gradient $\frac{du_e}{dx}$ is approximated by employing perturbation theory due to Oswatitsch (see Ref.14) resulting in a Mach number correction of the expression for incompressible flow.

The same perturbation theory can be used to approximate the heat flux away from the stagnation point using the series expansion developed by Frössling (Ref.5).

Cooling channel heat transfer. The heat transfer in a circular channel is analyzed by using the theoretical velocity profile of a fully developed flow in a pipe. First the shear stress along the wall is determined and then, in a second step, the result is used to formulate an expression for the heat transfer based on similarity of the momentum and energy boundary layer equations.

The shear stress along the wall of a pipe is written:

$$\tau_w = \frac{1}{8}\lambda\rho\overline{u}^2, \tag{11}$$

where λ is proportionality parameter to be determined. For a given relative roughness k_s/D of the pipe wall and given Reynolds number Re_D, defined as:

$$Re_D = \frac{\rho\overline{u}D}{\mu} \tag{12}$$

the Colebrook and White formula (Ref.11) is used to determine λ:

$$\frac{1}{\sqrt{\lambda}} = 1.74 - 2\log(2k_s/D + \frac{18.7}{Re_D\sqrt{\lambda}}). \tag{13}$$

Solution of this implicit equation for λ and substitution into Eq.(11) yields the shear stress along the wall, which can be non-dimensionalised using a friction coefficient formulation:

$$c_f' \equiv \frac{\tau_w}{\frac{1}{2}\rho\overline{u}^2}. \tag{14}$$

When we define the Stanton number as:

$$St = \frac{q_w}{\rho\overline{u}c_p(T_w - \overline{T})}, \tag{15}$$

the Prandtl-Taylor formula can be used to formulate the appropriate Reynolds analogy between the friction coefficient and the Stanton number (Ref.11):

$$St = \frac{\frac{1}{2}c'_f}{1 + 5\sqrt{\frac{1}{2}c'_f}(Pr - 1)}. \tag{16}$$

4.3 Computational Fluid Dynamics Analysis

For general complex three-dimensional configurations the Navier-Stokes equations can only be solved by means of discretisation and numerical solution, i.e., by means of Computational Fluid Dynamics (CFD). Several completely or partially NLR-developed CFD codes are available at NLR:

- ENFLOW: Multi-block structured grid approach
- FASTFLO: Hybrid prismatic/tetrahedral grid approach
- HEXADAP: Unsteady computational aerodynamics

Detailed chatacteristics of these codes are reviewed in Ref. 10. In addition, a commercially available code to compute gas turbine stages is available at NLR:

- Fine/Turbo (NUMECA): gas turbine flow simulation

All of these codes employ Finite Volume or Finite Element discretisation of the Navier-Stokes equations.

ENFLOW application To validate the computation of heat transfer to a turbine blade by ENFLOW, a 2D turbine cascade of the Von Karman Institute is considered. Experimental results are available (Ref. 1) in which both the pressure distribution along a blade, as well as the heat-transfer coefficient have been determined. The periodicity of the flow has also been verified.

An impression of the geometry, together with the employed grid of nearly 10,000 grid cells is given in figure 3a.

The grid is required to be periodic in the vertical (z) direction, which means that the grids along the upper and lower boundaries must be identical. This requirement together with the preference for an orthogonal grid in the near wake (to capture both the wake and shock properly, see figure 3b), lead to the particular block topology with a 'triangular' block next to the exit plane. The entrance and exit planes in the computations are placed at the exact locations where in the experiment entrance and exit conditions have been measured ($x/c_x = -1.487$ and $x/c_x = 1.433$, respectively, with $x = 0$ at the leading edge of the blade, and with c_x the chord length in x direction).

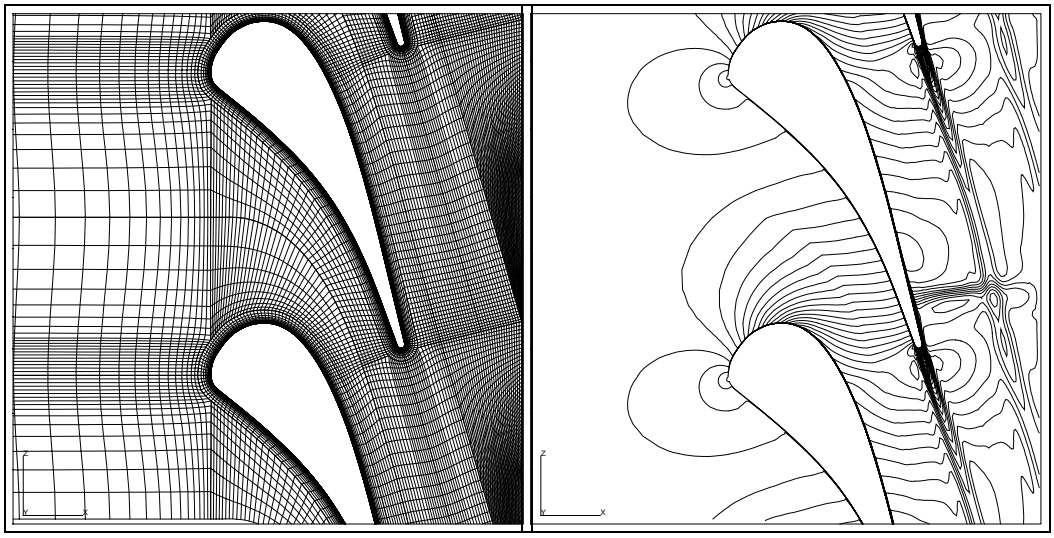

a) Computational grid *b) Lines of constant Mach number*

Fig. 3 Computed flow around VKI 2D turbine cascade, ($M_{\rm in} = 0.15$, $Re_{\rm in} = 2.4 \cdot 10^5$, $T_w/T_{\rm in} = 0.72$)

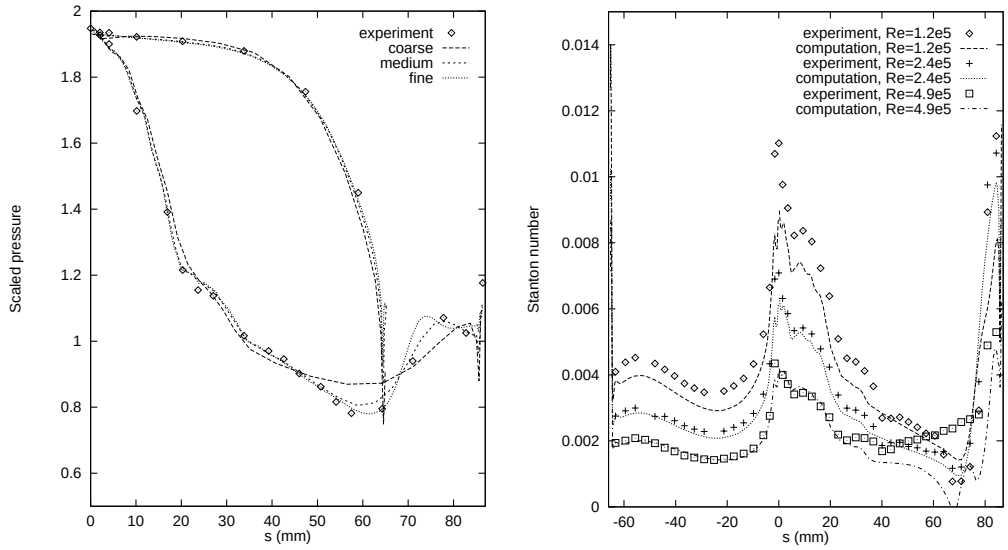

a) Scaled pressure, varying resolution *b) Stanton number*

Fig. 4 Scaled pressure $p/p_{\rm out}$ for $Re_{\rm out} = 1 \cdot 10^6$ and Stanton number for various Reynolds numbers as functions of arc length s for VKI 2D turbine cascade,($M_{\rm is,out} = 1.02$, adiabatic)

The computed pressure distribution compares well with the experimental values, see Fig. 4a.

The fine grid solution is also grid converged, with exception of the shock which might steepen further. The dependency of the heat transfer on the Reynolds number is shown in figure 4b. For each of the three Reynolds numbers, the transition has been set near to the experimental value,

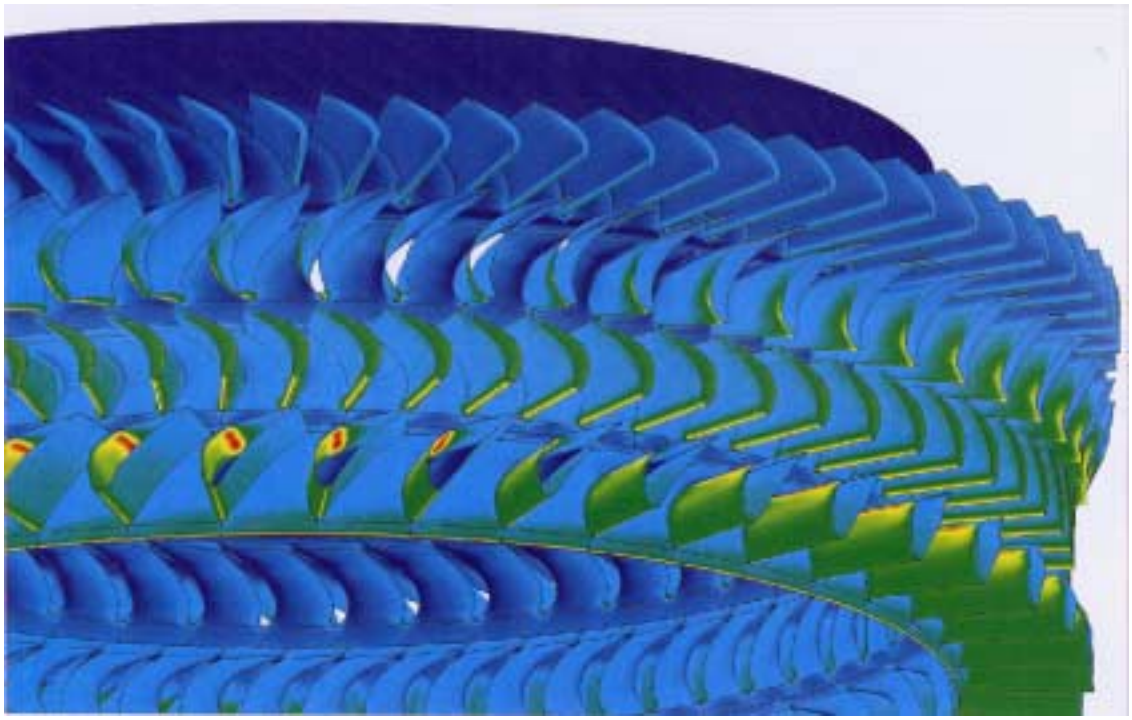

Fig. 5 Heat-transfer on two high-pressure turbine stages of the F100-PW-220 gas turbine engine, computed with Finite Volume Method

based on the distribution of the Stanton number.

NUMECA application The NUMECA code has been applied to two high-pressure turbine stages of the F100-PW-220 gas turbine engine to calculate the heat-transfer on the blade surfaces. Approximately 620,000 nodes have been used, while each node corresponds to seven degrees of freedom:

1. density,
2. momentum (three directions),
3. total energy,
4. turbulent kinetic energy, and
5. turbulent dissipation rate.

Fig. 5 shows the calculated heat transfer rate on the surfaces of the blades.

5 Heat Flow Analysis

The temperature distribution in a cooled gasturbine component depends on:

- the heat flux from the gas flow to the surface of the component which is determined by the heat transfer coefficient, the adiabatic wall temperature of the external flow and the wall temperature,
- the radiated heat flux (not employed in the present paper) determined by the coefficient of emissivity, the wall temperature and the environment radiation,
- the heat flux to the cooling channel flow from the cooling channel surface of the component which is determined by the heat transfer coefficient, the adiabatic wall temperature of the cooling channel flow and the wall temperature ,
- the heat flow in the structure of the gasturbine component determined by the heat conduction coefficient, the specific heat coefficient and the mass density.

5.1 Fourier Heat Equation

The heat conduction equation for a solid can be derived from the energy conservation law Eq. (6) by neglecting the velocity terms, yielding $E = e$, and assuming constant density and using the specific energy definition

$$e(T) = \int_0^T C(T)dT. \tag{17}$$

Then, employing the Fourier heat conduction law Eq. (8), we obtain

$$\rho C \frac{\partial T}{\partial t} - \frac{\partial}{\partial x^j} k \frac{\partial T}{\partial x^j} = 0. \tag{18}$$

Boundary conditions for the heat conduction equation typically consist of initial temperature distribution in the entire domain, and temperature and/or heat transfer rate prescription on the boundaries.

5.2 Asymptotic Heat Flow Analysis

Steady-state heat flow analysis For internally cooled cylinder exposed to a hot gas cross flow, see Fig. 6a, the temperature distribution along a line starting from the stagnation point in flow direction ($\phi = 0$ position), can be computed using asymptotic analysis. First the heat conduction equation Eq. (18) can be written in polar coordinates and then derivatives in axial and circumferential direction are assumed to be neglegible. For the single-layer configuration, see Fig. 6a, in the

limiting case of temperature independent conductivity the resulting equation is:

$$\frac{d^2T}{dr^2} + \frac{1}{r}\frac{dT}{dr} = 0. \tag{19}$$

The solution to this equation has the form:

$$T(r) = a\ln(r) + b, \tag{20}$$

with a and b constants to be determined from boundary conditions.

This result can be extended towards the multi-layer configuration, see Fig. 6b, where the cylinder wall consists of a number of layers with different material properties (see Fig. 6).

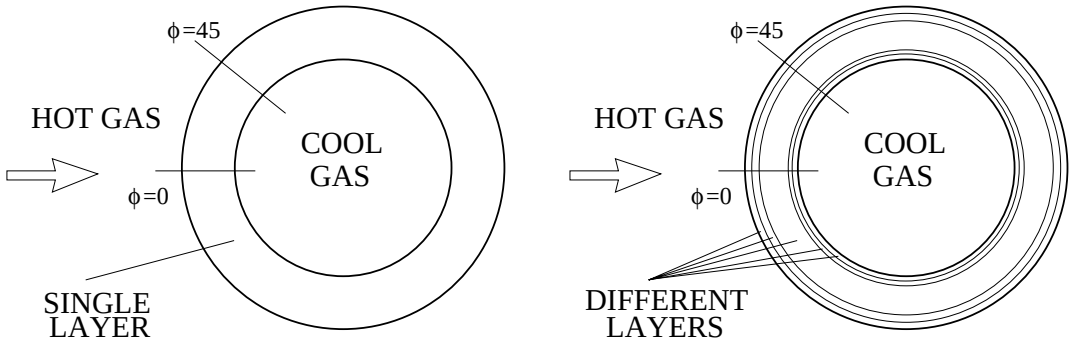

a) Single-layer configuration *a) Multi-layer configuration*

Fig. 6 Two different configurations of an internally cooled cylinder

Such analysis is useful for a detailed study on the effects of coated configurations. Let the i-th layer be defined by $r_{i-1} < r < r_i$, then the multi-layer solution to Eq. (19) is:

$$T(r) = a_i\ln(r) + b_i, \quad r_{i-1} < r < r_i, \tag{21}$$

with a_i and b_i constants to be determined from boundary conditions at the interfaces between layers. An example of this solution is presented in Fig. 7 for a 5-layer configuration including substrate material, thermal barrier coating and bond coating at the outer surface, and coating and oxyde-layer at the inner surface.

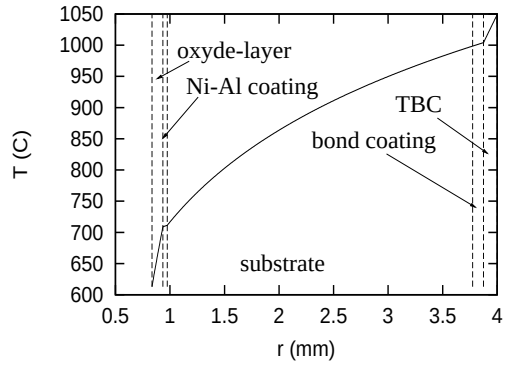

Fig. 7 Radial distribution of temperature in a 5-layer cylinder configuration

Time-accurate heat flow analysis The time dependent analogue of Eq. (19) in the limit of an asymptotically small wall-thickness compared to the radius is:

$$\frac{\rho C}{k}\frac{\partial T}{\partial t} - \frac{\partial^2 T}{\partial r^2} = 0. \tag{22}$$

Employing a heat transfer boundary condition at the outer boundary, using the Fay and Riddell formula presented in section 4.2, and an adiabatic or cooling-channel boundary condition at the inner boundary of the cylinder wall, using the formulas also presented in section 4.2, one can solve the boundary value problem by means of a series expansion:

$$T(r,t) = T(r,\infty) + \sum_{n=1}^{\infty} f_n(r) exp(\frac{-k\lambda_n^2 t}{\rho C}), \tag{23}$$

with

$$f_n(r) = A_n\, cos(\lambda_n r) + B_n\, sin(\lambda_n r). \tag{24}$$

Fig. 8 Computed temperature distributions in gas turbine blade including cooling channels

The constants λ_n, A_n and B_n can be determined from the boundary conditions and by employing the Sturm-Liouville theorem (Refs. 15 and 3).

5.3 Computational Heat Flow Analysis

At NLR computational heat flow analysis can be carried out using finite difference programs, e.g. ESATAN and NLR-developed codes, and finite element programs, e.g. MARC and B2000. MARC is a commercially available finite element program capable of non-linear heat flow and stress analysis. B2000 is a highly modular finite element program which is used as a testbed for advanced numerical algorithms. In the pilot phase all programs were used and it was decided to use MARC and B2000 for further investigations.

In the framework of several projects on gasturbine components transient as well as steady state heat flow analyses have been carried out with MARC. For most analyses heat transfer coefficients were used for heat flux boundary conditions. Also, steady-state analyses were carried out with specified wall temperatures as boundary conditions. A typical temperature computation result is presented in Fig. 8 showing computed temperature distributions in a gas turbine blade including cooling channels.

5.4 Heat Flow Experiments

Demonstrator experiments were carried out to validate the methods to calculate heat transfer and temperature distributions in an internally cooled or insulated hollow cylinder exposed to a hot

gas flow, see Fig. 6a. The test was executed using the NLR high temperature burner rig, where service conditions with respect to the temperature (max. $1875\,K$), heat-up and cool-down rates (up to $40\,K/s$) and gas velocity (max. $250\,m/s$) can be simulated. Also, pollution as SO_2 and artificial sea salt can be injected in the combustion chamber. The experiments were performed at temperatures between $875 - 1475\,K$, within a Mach range of 0.3 to 0.6 and with an internal cooling of the cylinder of 0, 45, and $90\,m/s$ airflow. The cylinder was made of $IN738$ and was not coated. The outer diameter was $20\,mm$, the wall thickness $4\,mm$.

The temperature distribution and (local) strains of the cylinder were recorded using thermocouples, which were placed inside the cylinder wall, an infrared camera, 2 pyrometers and a CCD camera. Fig. 9a shows an overview of the test set-up with the instrumentation, while Fig. 9b shows a closer

a) Overview *b) Operational*

Fig. 9 Burner rig test set-up with instrumentation

view of the test set-up in operation. The main result of the experiments is the time dependent temperature difference over the wall thickness during heat-up. An example is shown in Fig. 11 for a gas temperature of $875\,K$, a Mach number of 0.4 and an internal air flow of $90\,m/s$ at two angular positions, see also Fig. 6a.

5.5 Example of Heat Flow verification and validation

In this section an example of one of the finite difference methods mentioned in section 5.3 is presented.

Verification is obtained by comparison of the finite difference method with the time-acurate asymptotic analysis method presented in section 5.2. Fig. 10 shows such comparison in terms of the relative temperature error as a function if time and the number of grid points used. It is observed

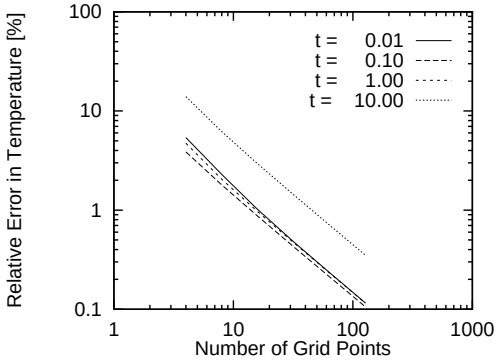

Fig. 10 Comparison between solutions obtained from analytical method and finite difference method as a function of time and number of grid points

that the error decreases uniformily with the number of grid points for all time instances plotted.

Validations is obtained from comparison of the finite difference method with data obtained from the physical experiment presented in section 5.4. Fig. 11 shows such comparison in terms of

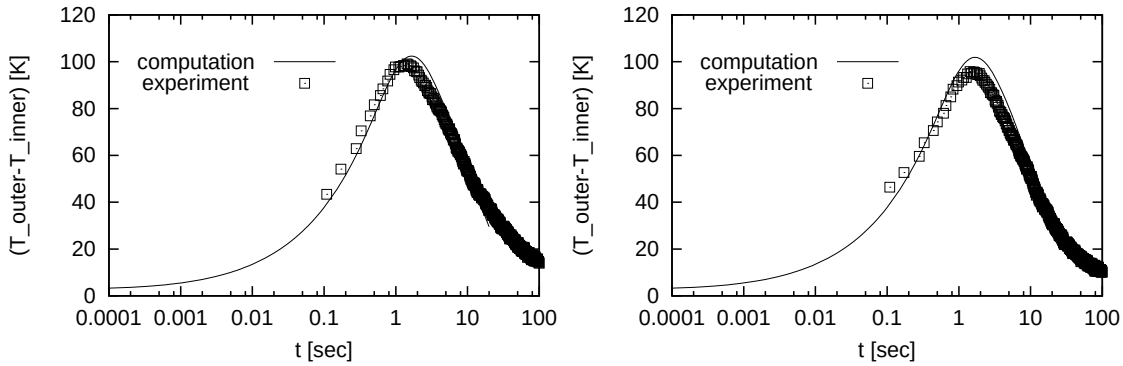

a) $\phi = 0°$ *b)* $\phi = 45°$

Fig. 11 Comparison of transient temperature differences between outer and inner boundary at two angular positions on single-layer cylinder obtained from 2D finite difference computations and measurements

the temperature difference between the outer and inner surface at two angular positions. Both at $\phi = 0°$ and at $\phi = 45°$ the agreement between the computational and experimental data is good.

6 Stress Analysis

The stresses in a (cooled) gasturbine component are associated with:

- thermal expansion, both instationary and steady-state,
- rotational speed,
- aerodynamic loads caused by the external and internal gas flows.

The temperature distributions and aerodynamic loads are obtained from the (in-house) numerical codes, see previous sections.

6.1 Navier-Cauchy Stress Equations

The solution of a structural problem must simultaneously satisfy the equilibrium equations, the compatibility requirements and the constitutive relations.

The equilibrium equations for the case where no external forces are present can be derived from the steady-state momentum conservation equations Eqs. (5) by neglecting the time-derivatives and the velocity terms. If there are external forces, the equilibrium equations are given by

$$\frac{\partial}{\partial x^j}\sigma^{ij} + F^i = 0 \tag{25}$$

The compatibility requirements are given in terms of strains. The strain equations define the relation between deformation and displacement. For a linear, homogeneous, isotropic material they are:

$$\epsilon^{ij} = \frac{1}{2}(\frac{\partial u^i}{\partial x^j} + \frac{\partial u^j}{\partial x^i}) \tag{26}$$

The constitutive relations define the relation between stress and deformation. For a linear, homogeneous, isotropic material they are given by:

$$\sigma^{ij} = \frac{\nu E}{(1+\nu)(1-2\nu)}\delta^{ij}\epsilon^{kk} + 2G\epsilon^{ij} \tag{27}$$

Substitution of (26) and (27) into (25) gives the Navier-Cauchy equations

$$\frac{\partial}{\partial^2 x^j}u^i + \frac{1}{1-2\nu}\frac{\partial}{\partial x^j}(\frac{\partial}{\partial x^i}u^j) + \frac{F^i}{G} = 0 \tag{28}$$

which can be solved to obtain the displacements. Boundary conditions for these equations typically consist of displacement restrictions and prescription of stress distribution on part of the outer boundary.

Non-linear material behavior: Creep and plasticity are examples of non-linear material behavior. In that case the constitutive relations (Eq. 27) are no longer linear. In the case of creep, strain is also a function of time, which must also be included in the constitutive relations.

Non-isotropic material behavior: Single crystal (SX) materials show anisotropic material behavior, which means that the constitutive relations are no longer symmetric. The general form is now

$$\sigma^{ij} = A^{ijkl}\epsilon^{kl} \tag{29}$$

where A is a 9x9 matrix. For an isotropic material the material behavior is fully described by two parameters (E and ν) whereas for an anisotropic material the number of parameters is much larger.

6.2 Asymptotic Stress Analysis

Steady-state stress analysis For the multi-layer cylinder configuration in Fig. 6 the stress and displacement distributions can be computed using asymptotic analysis and the temperature distribution Eq. (21) of section 5.2. Under the assumption of axially symmetric conditions there is no shear stress and we have the following result for the normal stresses σ_{rr}, $\sigma_{\theta\theta}$ and σ_{zz} in radial, circumferential and axial direction, respectively, and the radial displacement u in the i-th layer $r_{i-1} < r < r_i$:

$$\begin{aligned}
\sigma_{rr} &= -\frac{\alpha_i E_i}{1-\nu_i}\frac{1}{r^2}\int_{r_{i-1}}^{r}(T-1)r\,dr + \frac{E_i}{1+\nu_i}(\frac{C_{1i}}{1-2\nu_i} - \frac{C_{2i}}{r^2}),\\
\sigma_{\theta\theta} &= \frac{\alpha_i E_i}{1-\nu_i}\frac{1}{r^2}\int_{r_{i-1}}^{r}(T-1)r\,dr + \frac{E_i}{1+\nu_i}(\frac{C_{1i}}{1-2\nu_i} + \frac{C_{2i}}{r^2}) - \frac{\alpha_i E_i}{1-\nu_i}(T-1),
\end{aligned}$$

$$\begin{aligned} \sigma_{zz} &= -\frac{\alpha_i E_i}{1-\nu_i}(T-1) + \frac{2\nu_i E_i C_{1i}}{(1+\nu_i)(1-2\nu_i)} + C_3 E_i, \\ u &= \frac{1+\nu_i}{1-\nu_i}\frac{\alpha_i}{r}\int_{r_{i-1}}^{r}(T-1)r\,dr + C_{1i}r + \frac{C_{2i}}{r}, \end{aligned} \tag{30}$$

with the constants C_{1i}, C_{2i} and C_3 satisfying a linear system determined by the boundary conditions imposed on the inner and outer boundary of the cylinder and at the interfaces between the different material layers. It is noted that the present formulation is a generalisation of the single-layer cylinder configuration expressions derived in 13 and 2.

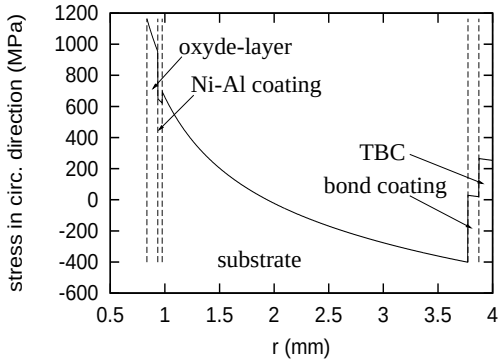

Fig. 12 Radial distribution of circumferential stress-component in a 5-layer cylinder configuration

Fig. 12 shows a typical result obtained from the asymptotic analysis, for a 5-layer configuration including substrate material, thermal barrier coating and bond coating at the outer surface, and coating and oxyde-layer at the inner surface, based on the calculated temperature distribution presented in Fig. 7.

6.3 Computational Stress Analysis

Computational stress analysis is primarily carried out using the previously mentioned Finite Element codes MARC and B2000, see section 5.3. Within the field of gas turbine investigations both quasi-steady-state computations as well as creep computations are performed.

A typical example of quasi-steady-state thermal stress computation is presented in Fig. 13, showing computed the thermal stress distribution in gas turbine blade including cooling channels as a reponse to the temperature distribution presented in Fig. 8.

On a much smaller physical scale a critical phenomenon is the potential delamination of thermal

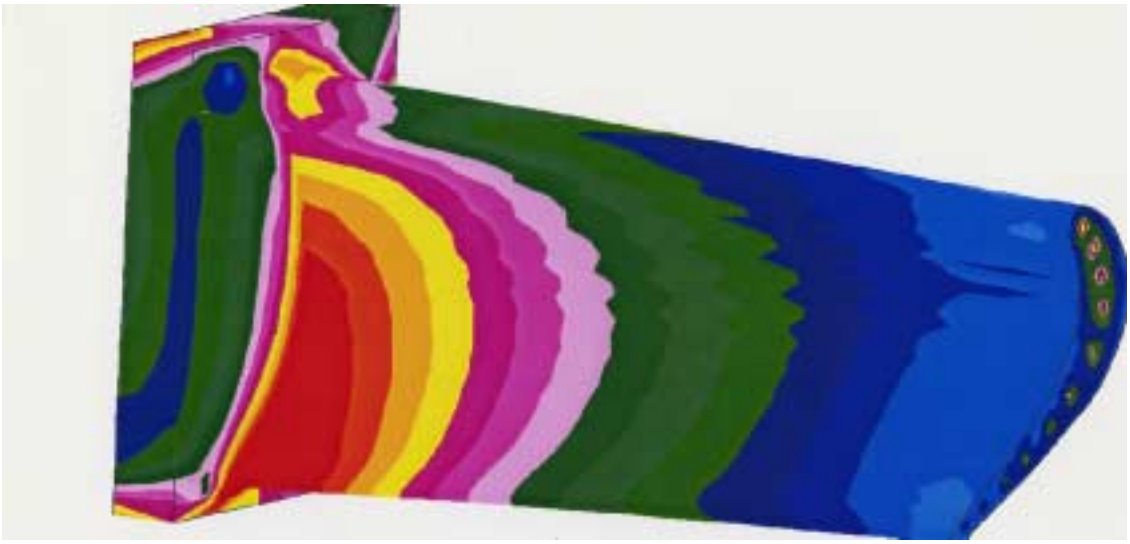

Fig. 13 Computed thermal stress distributions in gas turbine blade including cooling channels

barrier coating (TBC). A TBC is an insulating ceramic layer of material applied to components of gas turbines that are exposed to high thermal loads. The life of TBC's during service is limited due to thermal expansion mismatch stresses, interface roughness and bond coat oxidation. Delamination preferentially occurs parallel and adjacent to the interface with the bond coat.

Thermo-mechanical analysis of TBCs requires high-resolution stress analysis of the interface region. For this purpose a global-local model approach has been developed based on using a medium-resolution grid for a global solution to obtain boundary conditions on a high-resolution grid for a local solution. This global-local model approach has been employed successfully to investigate the influences on the stress distribution in this area due to interface roughness at the one hand, and of the presence of an oxidation layer between the bond coat and the top coat of a plasma-sprayed TBC at the other hand. Fig. 14a shows the FEM-mesh of the interface region. The shear strains near the free edge of a specimen after cooling from $1137^{\circ}C$ are shown in Fig. 14b. Just above the interface roughness peaks, in the region where delamination is normally observed, high shear stresses developed. The stresses increased with increasing top coat thickness. In comparison to non-oxidised bond coats, an interface oxidation layer resulted in higher interface stresses in the top coat.

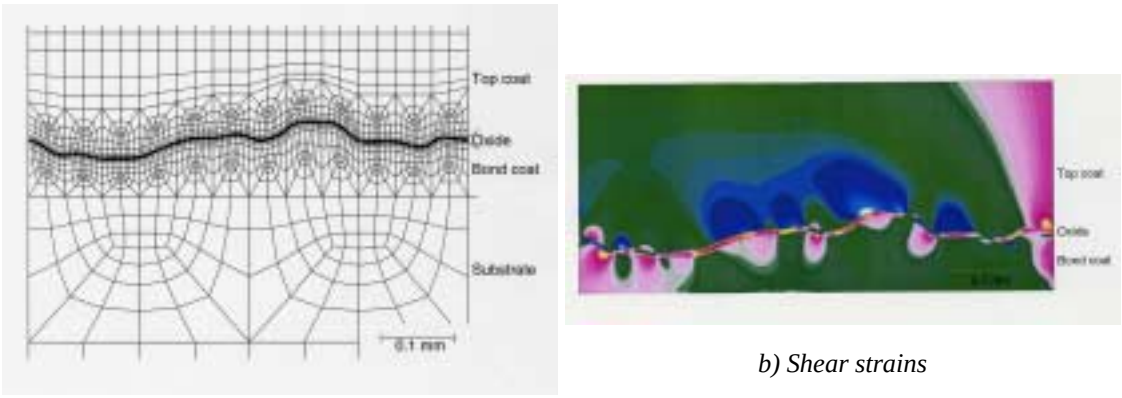

a) FEM-mesh

b) Shear strains

Fig. 14 FEM-mesh and shear strains near the free edge of a specimen after cooling from $1130\,^{\circ}C$

7 Life Assessment

The life consumption of a component can be thought of in terms of increasing damage. Different mechanisms can be responsible for the damage accumulation. Some well known mechanisms are:

- fatigue,
- creep,
- oxidation,
- dwell,
- corrosion,
- erosion, and
- fretting and wear.

The degree to which these mechanisms will influence the component's life depends primarily on the properties of the selected materials and the loading of the component. For example, a component operated at a high temperature under cyclic loading with a high minimum stress will experience damage due to fatigue as well as creep. In some cases the damage is more related to the properties of the fluid than to those of the component. Erosion for example is related to the direction of the solid particles in the flow. This report mainly focuses on the first three damage mechanisms, as these are the most important ones for gas turbine components.

Especially for the hot section of a gas turbine the flow properties like temperature and velocity are, directly or indirectly, responsible for the life. This illustrates the importance of the determination of the loads in the life prediction process.

The magnitude of the stress largely determines the damage in a component. However the opposite is also true, the damage can influence the stress. As a result of damage the local stiffness of a

component changes. This results in a redistribution of the load which in its turn gives a change in stress. Similar, but less pronounced, is the influence of the damage on the temperature, caused by changes in the flow and the heat conduction. In addition to this, external factors are influencing the component's life, like manufacturing and material defects, construction and maintenance errors and foreign object damage.

In order to assure an acceptable level of safety, airworthiness authorities have established a set of regulations, with which aircraft manufacturers have to comply. An essential issue within this context is the determination of the life of aircraft components.

There are two main approaches to determine the life of a critical component. The first approach, often refered to as Safe Life, aims to retire a component before a crack originates. The second approach, called Damage Tolerance, recognises the presence of material defects and aims to monitor crack growth and remove the component before the crack becomes critical. These approaches require different life prediction models. The first approach can be applied using total life models where the second approach requires more complex fracture mechanics models. Both model categories are treated in this chapter.

7.1 Phenomena and Equations

There is a wide variety of life prediction models. With respect to the approaches introduced above these models can be classified into one of the following categories:

- Total Life models
- Fracture mechanics models

It is convenient to introduce an abstract description of damage in terms of various contributions, and to unify time-driven mechanisms and cycle-driven mechanisms to some degree. Then, using this description, numerous examples of models associated with the two life prediction categories are presented below.

Damage description Let the damage be represented by a functional D. It is assumed that D can be written as a linear combination of various contributions:

$$D(S_1, S_2, ..., S_n, t) = \sum_{i=1}^{n} D_i(S_i, t). \tag{31}$$

In this equation the functions $S_i(t)$, $i = 1, 2, ..., n$, represent the loads of n different failure mechanisms and $D_i(S_i, t) > 0$, $i = 1, 2, ..., n$, represent n contributions to the total damage, at time t, each of them corresponding to a single mechanism.

The failure mechanisms can be divided in two types:

- **time**-driven mechanisms: the damage increases with time.
- **cycle**-driven mechanisms: the damage increases with number of cycles.

For **time**-driven mechanisms, damage accumulation is based on Robinson's rule where the partial damage D_i is given by the functional

$$D_i(S,t) = \int_0^t \frac{dD_i}{dt}(S(\tau))d\tau, \tag{32}$$

In this formulation it is required to model the **time**-derivatives $\frac{dD_i}{dt}(S)$.

For **cycle**-driven mechanisms, damage accumulation is based on the Palmgren-Miner rule which is defined in terms of cycles. Therefore we write Eq. (32) for the partial damage D_i in terms of cycles:

$$D_i(S,t) = \int_0^t \frac{dD_i}{dt}(S(\tau))d\tau = \int_0^t \frac{dD_i}{dN_i}(S(\tau))\frac{dN_i}{dt}(S(\tau))d\tau,$$

where $N_i(S)$ denotes the number of cycles as a function of time:

$$N_i(S,t) = \int_0^t \frac{dN_i}{dt}(S(\tau))d\tau. \tag{33}$$

In this formulation it is required to model the **cycle**-derivatives $\frac{dD_i}{dN_i}(S)$.

Total Life models The present functional formulation of damage accumulation can accomodate many of the total life prediction models described in the literature. Employment of the model requires two steps:

- identification of the mechanisms involved in the failure process
- definition of the expression(s) for $t_{f,i}(S_0)$ and/or $N_{f,i}(S_0)$.

When the mechanism is time-driven, the time-derivative is modeled as:

$$\frac{dD_i}{dt}(S_0) = \frac{1}{t_{f,i}(S_0)}, \tag{34}$$

where $t_{f,i}(S_0)$ is the failure time for a load S_0, i.e., $t_{f,i}(S_0)$ satisfies

$$D_i(S_0, t_{f,i}(S_0)) = 1. \tag{35}$$

When the mechanism is creep, then $t_{f,i}(S_0)$ is the creep rupture time at load S_0, which is obtained from the creep rupture curve for the material under consideration. In that case the load S_0 is a specific combination of stress and temperature (or equivalently, a certain value for the Larsson-Miller parameter P_{LM}).

When the mechanism is cycle-driven, the cycle-derivative is modeled as:

$$\frac{dD_i}{dN_i}(S_0) = \frac{1}{N_{f,i}(S_0)} \tag{36}$$

where the number of cycles to failure $N_{f,i}(S_0)$ is defined such that, for a load S_0, we have

$$D_i(S_0, N_{f,i}(S_0)/\frac{dN_i}{dt}(S_0)) = 1. \tag{37}$$

Here, $N_{f,i}(S_0)/\frac{dN_i}{dt}(S_0)$ represents the failure time associated with the load S_0. The functional description for $N_{f,i}(S_0)$ is obtained from material behavior data (e.g. S-N curves). Often an equation of the following type is used:

$$N_{f,i}(S_0) = A[q_i(S_0)]^{\alpha}, \tag{38}$$

where $q_i(S_0)$ is a representative mechanical quantity like the stress or inelastic strain range and A and α are constants.

A number of failure modes can be cast into Eq. (38) 6.

High cycle fatigue (HCF). Fatigue due to alternating elastic stresses. This is the failure mode for cold section blades and vanes.

- Basquin
  - $N_{f,1}$: Eq. (38) with $q = \Delta\sigma_{elastic}$.

High temperature low cycle fatigue (LCF). Failure modes of components in the HPC and HPT sections of a gasturbine. Fatigue and creep interact in this mode and therefore creep-fatigue models are applied:

- Manson-Coffin
  - $N_{f,1}$: Eq. (38) with $q = \Delta\varepsilon_{inelastic}$.
- Strain-range partitioning
  - $N_{f,1}$ (totally plastic): Eq. (38) with $q = \Delta\varepsilon_{pp} = F_{pp} * \Delta\varepsilon_{inelastic}$.
  - $N_{f,2}$ (totally creep): Eq. (38) with $q = \Delta\varepsilon_{cc} = F_{cc} * \Delta\varepsilon_{inelastic}$.
  - $N_{f,3}$ (plastic-creep): Eq. (38) with $q = \Delta\varepsilon_{pc} = F_{pc} * \Delta\varepsilon_{inelastic}$.
  - $N_{f,4}$ (creep-plastic): Eq. (38) with $q = \Delta\varepsilon_{cp} = F_{cp} * \Delta\varepsilon_{inelastic}$.
  - $N_{f,5}$ (elastic): Eq. (38) with $q = \Delta\varepsilon_e$.
- Ductility exhaustion
  - $N_{f,1}$(fatigue): Eq. (38) with $q = \Delta\varepsilon_{plastic}$ and $\alpha = 1$, while A represents the fatigue ductility (amount of plastic strain at failure).
  - $N_{f,2}$(creep): Eq. (38) with $q = \Delta\varepsilon_{creep}$ and $\alpha = 1$, while A represents the low band creep ductility.

Creep-rupture. Failure mode for the components in the combustor, e.g. liners. Over a large region creep strain rate depends linearly on stress and temperature.

- $t_{f,1}$: the rupture time as a function of stress and temperature, often in terms of the Larson-Miller parameter P_{LM}.

Oxidation. Failure mode for Thermal Barrier Coatings when combined with fatigue.

- Miller
  - $N_{f,1}$: Eq. (38) with $q = (1 - \frac{\Delta\varepsilon}{\Delta\varepsilon_f})(\frac{w_N}{w_c})^m + \frac{\Delta\varepsilon}{\Delta\varepsilon_f}$, where $\Delta\varepsilon$ is the applied strain range. This strain occurs when the TBC system heats up and it is caused by the difference in coefficient of thermal expansion for respectively the bondcoat and the topcoat. w_N is the total weight gain due to bondcoat oxidation in the thermal cycles, given by $\ln w_N(t) = \beta_0 + \beta_1 * \ln t$. Therefore the parameters in this model are the failure strain

range $\Delta\varepsilon_f$, the oxidation parameters β_0 and β_1, the critical weight gain w_c and the exponents m and b. These parameters have to be determined for the TBC system the model is applied upon.

Using these total life models, and thereby applying the Safe Life approach, two important assumptions are made: 1. The damage increment is not dependent on the existing damage. 2. There is no coupling between the different damage mechanisms. The only exception is Miller's oxidation model. In this model the damage increment is dependent on the amount of damage.

The equations to be used for$N_{f,i}$ and $t_{f,i}$ depend on the process responsible for the damage. A wide variety of equations is used but, however, research to improve these equations is an ongoing process.

Fracture Mechanics models Fracture Mechanics models are applied when the damage tolerance approach is used. In this approach the existence of a defect, in most cases represented by a crack, is recognised, and the growth of this defect during the life is predicted. The total life is consumed when the defect reaches a critical size. Within the original damage tolerance approach it is stated that the initial defect size is not smaller than the minimally detectible defect size (with a high probability of detection) given the inspection procedures employed during the manufacturing process. This results in large (conservative) initial defect sizes. Using the models discussed later in this section the growth of the defect to a critical value is calculated. After a service period of, for example, 50% of the calculated life, the component is expected. If no defect is found the component can be kept in service for another period. This approach is prefered to the safe life approach since the damage accumulation is described in terms of measurable quantities. Practical application is possible only when firstly the predicted life is long enough to keep the number of inspections limited, and when secondly models are available which predict the life with sufficient accuracy.

In recent years a lot of research has been conducted on this subject, resulting in a large number of expressions, each appropriate for a certain material or application. A summary of crack growth prediction methods is given below where we have chosen to use the conventional notation; a represents some characteristic dimension of the crack under consideration, while each of the methods provides expressions for the crack-growth rate either in terms of the time-derivative$\frac{da}{dt}$ or in terms of the cycle-derivative $\frac{da}{dN}$. This formulation is completely compatible with the functional D described above.

FNK, the Forman, Newman and De Koning equation 9. This expression is used in the crack growth prediction program NASGRO. It accounts for crack closure and stress ratio effects. The mechanism is limited to fatigue.

$$(\frac{da}{dN}) = C\,[\frac{1-f}{1-R}\Delta K]^n\,[1-\frac{\Delta K_{th}}{\Delta K}]^p\,[1-\frac{\Delta K}{(1-R)\Delta K_c}]^{-q}. \tag{39}$$

In this equation ΔK is the stress intensity factor range, a loading parameter, incorporating effects of applied remote stress, actual crack length and specimen geometry. Furthermore R is the stress ratio and f the crack closure coefficient. The remaining parameters are material dependent coefficients.

MSE, the General Electric Modified Sigmoidal Equation (MSE) model 17. Fatigue and creep, integrated into a single expression for da/dN.

$$(\frac{da}{dN}) = e^A\,[\frac{\Delta K}{\Delta K^*}]^B\,[\ln\frac{\Delta K}{\Delta K^*}]^C\,[\ln\frac{\Delta K_c}{\Delta K}]^Q. \tag{40}$$

This model does not have a clear physical background. It is based on the knowledge that da/dN as a function of ΔK has a sigmoidal shape. Except for the stress intensity factor range ΔK all parameters are material dependent coefficients.

SINH, the Pratt & Whitney Hyperbolic Sine Equation model 17. Fatigue and creep, integrated into a single expression for da/dN.

$$\log(\frac{da}{dN}) = C_1\sinh[C_2(\log(\Delta K)+C_3)]+C_4. \tag{41}$$

This model is also based on fitting da/dN as a function of ΔK.

A creep crack growth model controlled by C^*, the energy rate integral, which is a quantity similar to the J-integral under fully plastic behaviour. C^* incorporates applied load, crack length and

geometry effects.

$$(\frac{da}{dt}) = AC^{*m}, \tag{42}$$

A and m are material coefficients in 17, $A = \frac{3}{\varepsilon_f}$ and $m = 0.85$, where ε_f is the uni-axial creep ductility.

Combined method. A simple combined creep-fatigue model is presented in 18 where,

$$(\frac{da}{dt}) = (\frac{da}{dN})_{fat.}(\frac{dN}{dt}) + (\frac{da}{dt})_{creep}. \tag{43}$$

The fatigue contribution is modeled as

$$(\frac{da}{dN})_{fat.} = C\Delta K^n, \tag{44}$$

where again ΔK is the stress intensity factor range, and C and n are material dependent coefficients. The creep contribution is modeled as

$$(\frac{da}{dt})_{creep} = b[\frac{K^2}{t}]^p, \tag{45}$$

where K is the stress intensity factor at hold time and t is time. The other parameters are material dependent coefficients. This relatively simple model is valid for short hold times. For larger hold times C^* should be used instead of K to calculate the creep contribution.

7.2 Underlying assumptions

A number of assumptions has been used during development of most of the above formulated models, including:

- The damage increment is not dependent on the existing damage, or in other words: the influence of the damage on the stress distribution is neglected. This assumption leads in some cases to conservative life predictions. For multiple load path structures the damage decreases the local stiffness of the construction, causing the load to decrease. If this is

neglected in the analysis, conservative life predictions are obtained. There are two points to note however:

(a) the decrease in local stiffness causes an increase in load at other locations, where damage could occur (MSD).

(b) for crack initiation the mentioned simplification is quite realistic. The crack lengths are too small to effect the stress distribution and no stiffness decrease is caused.

- The interaction between the different failure mechanisms is neglected (except for the strain range partitioning method). This implies that, in some cases, the damage at failure is not 1, but has a larger or smaller value.

7.3 Computational Life Analysis

A number of codes is available at NLR:

- FATIGUE: developed to carry out life predictions based on fatigue models. It requires a load sequence, material properties and a relation between load and number of cycles to failure (S,N-curve) as input. Furthermore it is (will be) possible to make a choice between different lifing models (Linear Damage Rule, Strain-range Partitioning, Oxidation-based model for Thermal Barrier Coatings, lapjoint analysis, etc.)
- NASGRO and CRAGRO: crack growth prediction programs. They require a load sequence, material properties and a K-solution as input. The K-solution gives the relation between ΔK and crack length and translates the applied remote stress to the local stresses in the crack tip region, which cause the crack growth.

7.4 Life Experiments

For all the models, a (large) number of parameters has to be determined before a life assessment can be done. For a limited number of cases literature values are available. If this is not the case, experiments have to be done to determine the parameters.

Recently, experiments were done to determine the parameters in an oxidation-based life prediction model, included within the FATIGUE code, for Thermal Barrier Coatings (TBC). The results were used to predict the life of thermal shock and thermal cycling tests carried out at the University of Technology of Eindhoven. The experiments were performed on a TBC system consisting of Hastelloy X substrate, coated with a NiCrAlY bondcoat and a plasma sprayed Y_2O_3 stabilised ZrO_2 top coat.

The thermal shock (furnace) tests consist of cyclic heat-up and cool-down of the samples, with four different cycle times (1, 2, 8 and 24 hrs) at two different temperatures (1000 and 1100°C). These

tests give information about the oxidation behavior of the system and about the life, determined by the combination of fatigue and oxidation.

The results of the furnace tests are shown in Fig. 15a, where the number of cycles to failure is plotted versus the cycle length. It is observed from Fig. 15a that a larger cycle length induces a

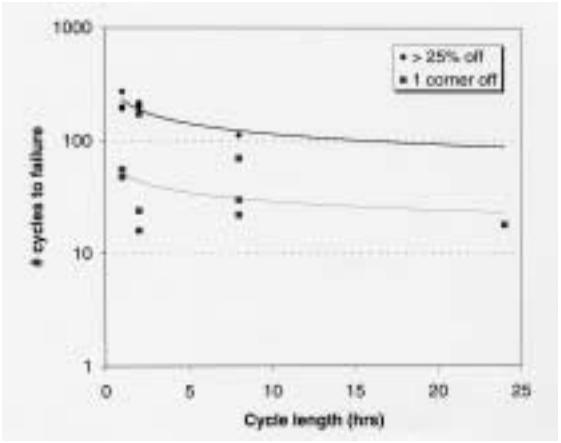

a) Number of cycles to failure

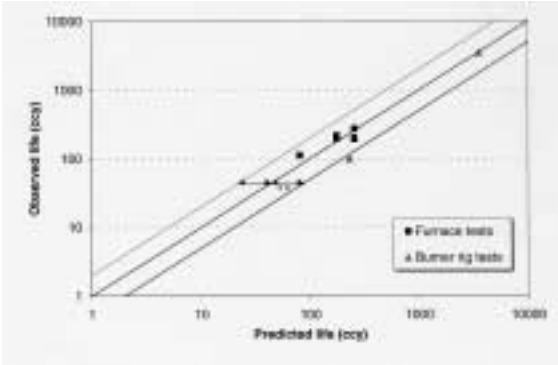

b) Predicted and observed life

Fig. 15 Experimental data obtained from furnace and burner rig tests compared to life prediction model

smaller number of cycles to failure. This can be attributed to the increasing influence of bond coat oxidation for the longer cycles.

The parameters for the life prediction model were determined from the experiments and the coating life was predicted for several cycle times. The results are shown in Fig. 15b. Most predictions fall within a factor of 2 scatterband which is a well-accepted range for life prediction. The prediction of the thermal cycling test on the burner rig is not very good. The bond-coat/top-coat interface temperature, however, was higher than the 1100° assumed in the model leading to an overprediction of the number of cycles to failure.

8 Conclusions

A review is presented concerning activities towards integrated analysis of gas turbine components for life prediction, conducted at the National Aerospace Laboratory NLR in the Netherlands.

Key elements are the multi-disciplinary frame-work including Engine System Performance, Fluid Dynamics Analysis, Heat Flow Analysis, Stress Analysis and Life Assessment, and the comple-

mentary approach consisting of Asymptotic Analysis, Numerical Analysis and Physical Experiments. Each of the disciplines is addressed in some detail on the level of at least two members of the complementary approach. While discussing the methods used, numerous applications are presented including verification and validation comparisons between members of the complementary approach.

9 References

1. T. Arts, M. Lambert de Rouvroit and A.W. Rutherford, *Aero-Thermal Investigation of a Highly Loaded Transonic Linear Turbine Guide Vane Cascade,* Technical Note 174, Von Karman Institute for Fluid Dynamics, 1990.
2. B.A. Boley and J.H. Weiner, *Theory of Thermal Stresses*, Dover Publications, 1985.
3. R. Courant and D. Hilbert, *, Methods of Mathematical Physics*, Volume I, John Wiley and Sons, 1989.
4. J.A. Fay F.R. Riddell, *Theory of Stagnation Point Heat Transfer in Dissociated Flow,* Journal of the Aeronautical Sciences, 25(2):73–85, 1958.
5. N. Frössling, *Evaporation, Heat Transfer, and Velocity distribution in Two-Dimensional and Rotationally symmetrical Laminar boundary-Layer Flow*, Technical Memorandum 1432, NACA, 1958.
6. T. Goswami, *Private communication*, Cessna Aircraft Company, 1999.
7. W.D. Hayes and R.F. Probstein, *Hypersonic Flow Theory*, Academic Press, 1959.
8. Larsen, J.M. *Cumulative damage modeling of fatigue crack growth in turbine engine materials*, Eng. Fracture Mechanics, 22(1985), 4, 713-730.
9. R.G. Forman and J.C. Newman, *Fatigue crack growth computer program "NASGRO"*, User's manual, NASA, Houston, 1996.
10. B. Oskam and J.W. Slooff, *Recent Advances in Computational Aerodynamics at NLR,* AIAA 98-0138, January 12-15, 1998/ Reno, NV
11. H. Schlichting, *Boundary-Layer Theory*, Seventh Edition, McGraw-Hill, 1979.
12. Spiekhout, D.J. *F-16 loads / usage monitoring*, NLR TP 98172, National Aerospace Laboratory, Amsterdam, 1998.
13. S.P. Timoshenko and J.N. Goodier, *Theory of Elasticity*, McGraw-Hill, international edition, 1970.
14. M. Van Dyke, *Perturbation Methods in Fluid Dynamics*, The Parabolic Press, Stanford, California, 1975.
15. C.R. Wylie and L.C. Barrett, *Advanced Engineering Mathematics*, McGraw-Hill, 1982.

16. W.P.J. Visser, *GSP, A Generic Object-Oriented Gas Turbine Simulation Environment*, ASME-2000-GT-0002.
17. G.F. Harrison and P.H. Tranter, *Defects and their effects on the integrity of nickel based aeroengine discs*, presented at 74th AGARD Symposium, Greece, 1992
18. A. Saxena and R.S. Williams, *A model for representing and predicting the influence of hold time on fatigue crack growth behavior atelevated temperature*, ASTM STP 743, 1981, 86-99.